Electronic Supplementary Information (ESI) for

Structure-property relationships for 1,7-diphenoxy-perylene bisimides in solution and in the solid state

Ángel J. Jiménez,[a] Mei-Jin Lin,[a] Christian Burschka,[a] Johannes Becker,[b] Volker Settels,[b] Bernd Engels,[b] and Frank Würthner*[a]

[a]*Universität Würzburg, Institut für Organische Chemie and Center for Nanosystems Chemistry, Am Hubland, 97074 Würzburg, Germany. Fax: +49/931/31-84756 Tel: +49/931/31-85340; E-mail: wuerthner@chemie.uni-wuerzburg.de*

[b]*Universität Würzburg, Institut für Physikalische und Theoretische Chemie, Am Hubland, 97074 Würzburg, Germany.*

Table of Contents:

1. Materials and Methods

Ortho-cresol, 2,6-dimethylphenol, 2,6-diisopropylphenol, potassium carbonate (≥ 99%) and *N*-methyl-2-pyrrolidone (NMP, 99.5%) were obtained from commercial suppliers. All chemicals and reagents were used as received unless otherwise stated. NMP was fractionally distilled prior to use and potassium carbonate was dried under vacuo at 100 °C for 24 h. *N*,*N*′-Dicyclohexyl-1,7-dibromoperylene-3,4:9,10-tetracarboxylic acid bisimide (**2**), reference compound *N*,*N*′-dicyclohexyl-3,4:9,10-tetracarboxylic acid bisimide (**4a**), *N*,*N*′-dicyclohexyl-1,7-diphenylperylene-3,4:9,10-tetracarboxylic acid bisimide (**4b**), and *N*,*N*′-dicyclohexyl-1,7-diphenylphenoxyperylene-3,4:9,10-tetracarboxylic acid bisimide (**4f**) were prepared according to literature procedures.[S1] Flash column chromatography was performed using silica gel (Si_{60}, mesh size 40-63 μm) from Merck. NMR spectra were recorded with a Bruker Avance 400 MHz instrument. Chemical shifts are given in parts per million (ppm) and referred to TMS as internal standard. ^{1}H coupling constants *J* are given in Hertz (Hz). MALDI-TOF mass spectra were recorded on an Autoflex II from Bruker Daltonics spectrometer. ESI-TOF mass spectra were recorded on a Bruker Daltonics micrOTOF focus instrument.

All the solvents used for the spectroscopic measurements were of spectroscopic grade (Uvasol®) and were used without further purification. The UV/Vis spectra were recorded on a Perkin Elmer PE 950 spectrometer equipped with a PTP-1 Peltier element for temperature control and corrected against the reference solution. The fluorescence spectra were recorded with a PTI QM-4/2003 instrument. All fluorescence measurements were performed under ambient conditions and corrected against photomultiplier and lamp intensity. The fluorescence quantum yields were determined as the average value for three different excitation wavelengths using *N*,*N*'-di(2,6-di-isopropylphenyl)-perylene-3,4:9,10-tetracarboxylic acid bisimide as reference (Φ_f = 1.00 in dichloromethane[S2]) by applying high dilution conditions (A < 0.05). Solid state absorption spectra of PBIs **4a** and **4b** were determined by applying the Kubelka-Munk theory to reflectance spectra of trituration of PBIs in $BaSO_4$ measured with a Lambda 950 UV/Vis/NIR spectrometer of Perkin Elmer equipped with an integrating sphere. Absolute fluorescence quantum yields were

determined on a Hamamatsu Absolute PL Quantum Yield Measurement System CC9920-02. The system is made up of an excitation source that uses a 150 W CW Xenon light source, a monochromator (250-700 nm, FWHM 10 nm), an integrating sphere, and a multi-channel spectrometer capable of simultaneously measuring multiple wavelengths between 300 and 950 nm and counting the number of absorbed and emitted photons.

2. Synthesis of PBIs

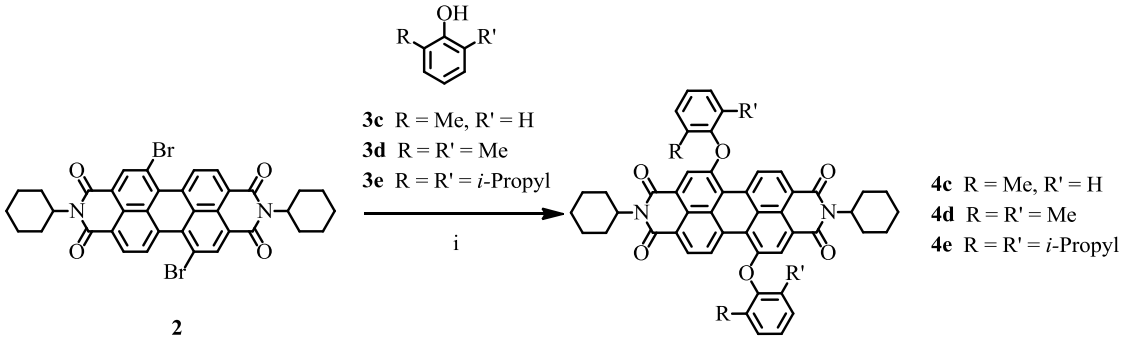

Procedure: To a degassed solution of PBI **2** (0.35 g, 0.49 mmol) and potassium carbonate (200 mg, 2.30 mmol) in dry NMP (20 mL) under argon, excess amounts of *ortho*-cresol **3c**, 2,6-dimeyhylphenol **3d**, or 2,6-diisopropylphenol **3e** (1.20 mmol) were added and the mixture was stirred at 120 °C for 3 h. After being cooled to room temperature, the reaction mixture was slowly dropped into 250 mL of 1N HCl under stirring. The solid material was separated by filtration and then washed successively with water (3 × 30 mL) and methanol (3 × 30 mL). The crude product was purified by column chromatography on silica gel using CH_2Cl_2 as an eluent and afforded red solid PBIs **4c, 4d** and **4e** in 87%, 74% and 88% yield, respectively.

PBI **4c**: M.p.: 399 °C; ^{1}H NMR (400 MHz, CD_2Cl_2, ppm): δ = 9.66 (d, *J* = 8.0 Hz, 2H), 8.54 (d, *J* = 8.0 Hz, 2H), 8.08 (s, 2H), 7.43 (dd, *J* = 1.0 Hz, 2H), 7.3-7.2 (m, 4H), 7.02 (dd, *J* = 1.0 Hz, 2H), 5.0-4.9 (m, 2H), 2.5-2.4 (m, 4H), 2.36 (s, 6H), 1.9-1.8 (m, 4H), 1.7-1.6 (m, 6H), 1.4-1.3 (m, 4H), 1.3-1.2 (m, 2H). ^{13}C NMR (100 MHz, $CDCl_3$, ppm): δ = 163.8, 163.4, 155.7, 152.7, 133.4, 132.3, 130.0, 129.9, 129.3, 128.8, 128.0, 125.7, 124.7, 124.3,

122.6, 122.5, 121.7, 120.3, 54.0 29.1, 26.5, 25.4, 16.2. ESI-TOF-MS, calculated for $C_{50}H_{42}N_2O_6$: 766.3043; found: *m/z* = 766.3112.

PBI **4d**: M.p.: 232 °C; ^{1}H NMR (400 MHz, CD_2Cl_2, ppm): δ = 9.78 (d, *J* = 8.0 Hz, 2H), 8.51 (d, *J* = 8.0 Hz, 2H), 7.81 (s, 2H), 7.22-7.16 (m, 6H), 4.91-4.83 (m, 2H), 2.34-2.34 (m, 4H), 2.12 (s, 12H), 1.80-1.77 (m, 4H), 1.63-1.60 (m, 6H), 1.39-1.29 (m, 6H). ^{13}C NMR (100 MHz, $CDCl_3$, ppm): δ = 164.1, 163.7, 155.9, 150.9, 134.0, 131.5, 130.1, 129.7, 129.6, 126.7, 124.9, 124.8, 122.9, 121.4, 118.5, 54.0, 29.4, 26.9, 25.9, 16.5. ESI-TOF-MS, calculated for $C_{52}H_{46}N_2O_6$: 794.3356; found: *m/z* = 794.3428.

PBI **4e**: M.p.: 198 °C; ^{1}H NMR (400 MHz, CD_2Cl_2, ppm): δ = 9.87 (d, *J* = 8.0 Hz, 2H), 8.57 (d, *J* = 8.0 Hz, 2H), 7.94 (s, 2H), 7.43-7.38 (m, 6H), 4.97-4.90 (m, 2H), 3.07-2.99 (m, 4H), 2.52-2.42 (m, 4H), 1.87-1.84 (m, 4H), 1.71-1.68 (m, 6H), 1.43-1.39 (m, 6H), 1.23 (d, *J* = 8.0 Hz, 12H), 1.11 (d, *J* = 8.0 Hz, 12H). ^{13}C NMR (100 MHz, CD_2Cl_2, ppm): δ = 164.1, 163.6, 157.1, 147.7, 141.9, 134.2, 129.9, 129.7, 129.2, 127.5, 125.6, 124.8, 124.6, 122.9, 121.0, 118.9, 54.1, 29.4, 27.9, 26.9, 25.9, 24.9, 22.7. ESI-TOF-MS, calculated for $C_{60}H_{62}N_2O_6$: 906.4608; found: *m/z* = 906.4598.

3. Single Crystal X-ray Analysis

Single crystals suitable for X-ray diffraction were obtained by dissolving the PBIs **4d** and **4e** in a mixture of CH_2Cl_2/EtOH = 90:10, followed by slow evaporation of the solvents (for single crystal data of PBI **4f**, see ref. S1c and CCDC 901365). Crystal data were collected on a Bruker X8APEX-II_KAPPA diffractometer with a CCD area detector and multi-layer mirror monochromated $Mo_{K\alpha}$ radiation. The structure was solved using direct methods (SHELXS), expanded using Fourier techniques and refined with SHELXL.[S3] Hydrogen atoms were included in structure factors calculations at idealized positions and refined using a riding model.

Crystal data for PBI **4d**: $C_{52}H_{46}N_2O_6 \cdot 0.5\ CH_2Cl_2$; M_r = 837.37, 0.2x0.2x0.1 mm^3, monoclinic space group *C2/c*, *a* = 22.8894(13) Å, *b* = 12.5211(6) Å, *c* = 15.4873(7) Å, β = 90.723(3)°, *V* = 4438.3(4) $Å^3$, *Z* = 4, *T* = 100(2) K. The unit cell contains 4 PBI molecules positioned on a crystallographic centre of symmetry, therefore Z =4, and furthermore 4 isolated regions (voids) with additional electron density, positioned each about a crystallographic 2-fold axis. This additional density could only partly be modelled as discrete atomic sites (*GooF*(F^2) = 1.128, R_1 = 0.073, wR^2 = 0.229 for I>2σ(I) and was attributed to disordered solvent of ½ CH_2Cl_2 per void. This formula $C_{52}H_{46}N_2O_6 \cdot 0.5\ CH_2Cl_2$ leads to the derived constants ρ_{calcd} = 1.253 $g \cdot cm^{-3}$, μ = 0.139 mm^{-1}, *F*(000) = 1764.

At this stage further additional electron density could still be found in difference fourier maps. So the "squeeze" procedure with PLATON[S4] was applied to calculate the contribution to the diffraction from this region, which found 4 voids in the cell, each with a volume of 127 $Å^3$, each occupied by 31 electrons. Compared to 42 electrons per molecule of CH_2Cl_2 this finding leads to a different sum formula of the investigated compound namely $C_{52}H_{46}N_2O_6 \cdot 0.74$ (CH_2Cl_2), which means there are 0.74 disordered solvent molecules per void.

Final refinements where calculated from filtered intensity data with masked out regions of the disordered electron density: $GooF(F^2) = 1.066$, $R_1 = 0.0585$, $wR^2 = 0.1722$ for I>2σ(I), $R_1 = 0.0692$, $wR^2 = 0.1808$ for all data, 4537 independent reflections [2 θ ≤ 52.84°] and 294 parameters.

Crystal data for PBI **4e**: $C_{60}H_{62}N_2O_6$; $M_r = 907.12$, red block, 0.28×0.17×0.10 mm^3, orthorhombic space group $Pna2_1$, $a = 22.956(2)$ Å, $b = 9.4115(19)$ Å, $c = 22.7754(8)$ Å, $V = 4920.7(11)$ Å^3, $Z = 4$, $\rho_{calcd} = 1.224$ g·cm^{-3}, $\mu = 0.078$ mm^{-1}, $F(000) = 1936$, $T = 100(2)$ K, $GooF(F^2) = 1.065$, $R_1 = 0.0537$, $wR^2 = 0.1315$ for I > 2σ(I), $R_1 = 0.0661$, $wR^2 = 0.1382$ for all data, 10041 independent reflections [2 θ ≤ 52.74°] and 725 parameters, 263 restraints. The fairly large number of restraints had to be applied to model disordered *i*-propyl groups and a disordered N-hexyl group with physically sensible parameters.

A second phase of PBI **4e** could be observed for some crystals which included CH_2Cl_2 from the same solvent mixture of CH_2Cl_2/EtOH = 90:10. Crystal data were collected on a 3 circle Rigaku CCD diffractometer at room temperature with a sealed molybdenum tube and graphite monochromator.

Crystal data for PBI **4e**: $(C_{60}H_{62}N_2O_6 \cdot 0.89\ (CH_2Cl_2))$; $M_r = 992.04$, red block, 0.36×0.32×0.26 mm^3, monoclinic space group $P2_1/n$, $a = 13.495(3)$ Å, $b = 14.896(3)$ Å, $c = 26.835(5)$ Å, $V = 5326.8(19)$ Å^3, β=99.08(2), $Z = 4$, $\rho_{calcd} = 1.237$ g·cm^{-3}, $\mu = 0.175$ mm^{-1}, $F(000) = 2104$, $T = 293(2)$ K, $GooF(F^2) = 1.326$, $R_1 = 0.1354$, $wR^2 = 0.2393$ for I>2σ(I), $R_1 = 0.1537$, $wR^2 = 0.2485$ for all data, 7622 independent reflections [2 θ ≤ 46.5°] and 688 parameters, 128 restraints. The fairly large number of restraints had to be applied to model disordered *i*-propyl groups, a disordered *N*-cyclohexyl group and a partially occupied solvent molecule with physically sensible parameters.

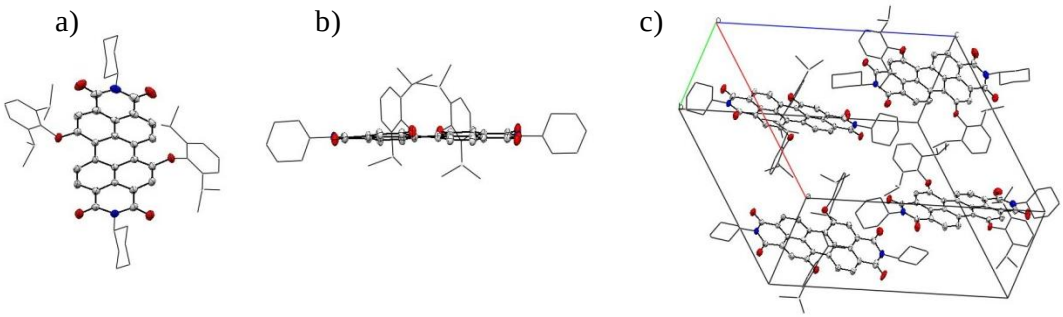

Fig. S1 Molecular structure in front view (a) and in side view (b), and molecular packing (c) of PBI **4e** in the solvent-free single crystal.

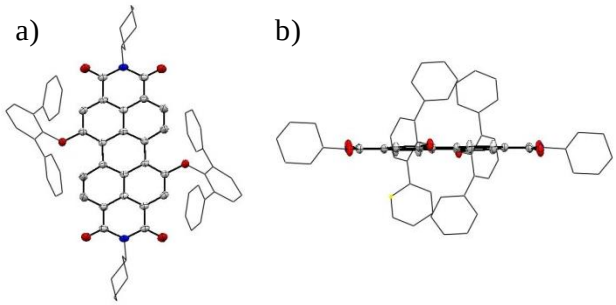

Fig. S2 Molecular structure in front view (a) and in side view (b) of PBI **4f** (from ref. S1c).

Crystallographic data for the three new crystal structures (one for **4d**, two for **4e**) have been deposited with the Cambridge Crystallographic Data Center as supplementary publication no. CCDC 952111-952113. These data can be obtained free of charge from The Cambridge Crystallographic Data Centre *via* www.ccdc.cam.ac.uk/data_request/cif.

4. Absorption and Fluorescence Spectra in Solution and in the Solid State

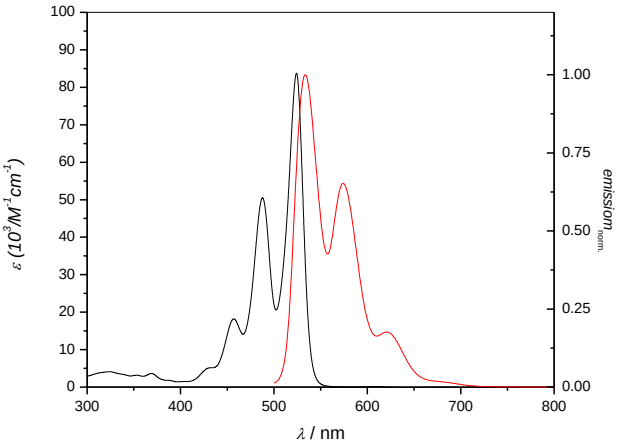

Fig. S3 UV/Vis absorption and emission spectra (both at a concentration of 7.0×10^{-6} M) of PBI **4a** in dichloromethane at room temperature.

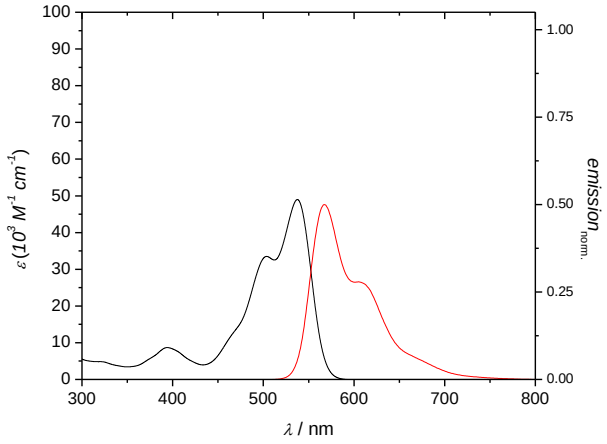

Fig. S4 UV/Vis absorption and emission spectra (both at a concentration of 2.0×10^{-5} M) of PBI **4b** in dichloromethane at room temperature.

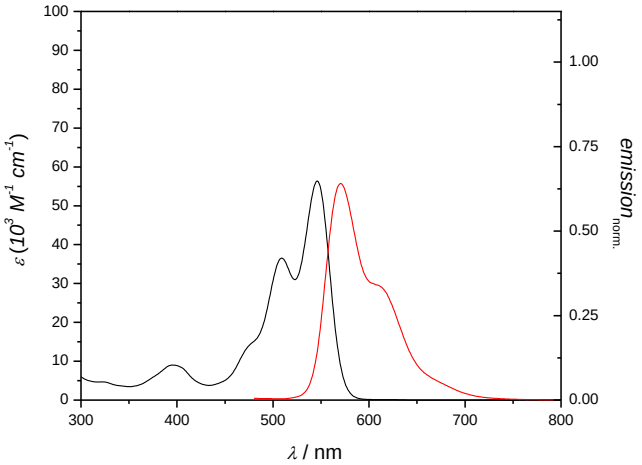

Fig. S5 UV/Vis absorption and emission spectra (both at a concentration of 1.9×10^{-5} M) of PBI **4c** in dichloromethane at room temperature.

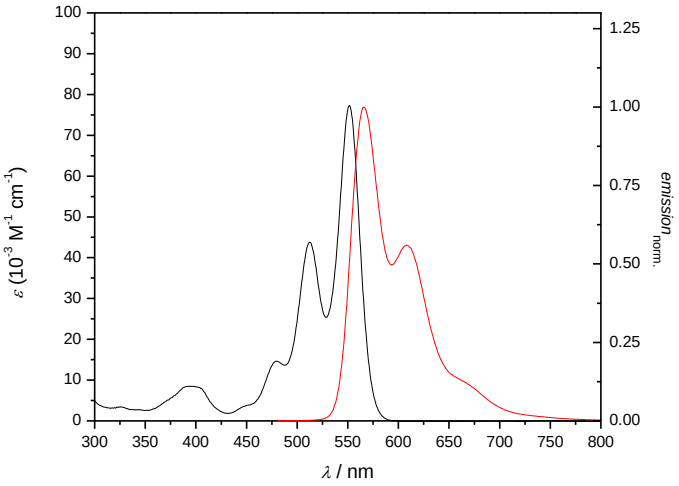

Fig. S6 UV/Vis absorption and emission spectra (both at a concentration of 4.0×10^{-6} M) of PBI **4d** in dichloromethane at room temperature.

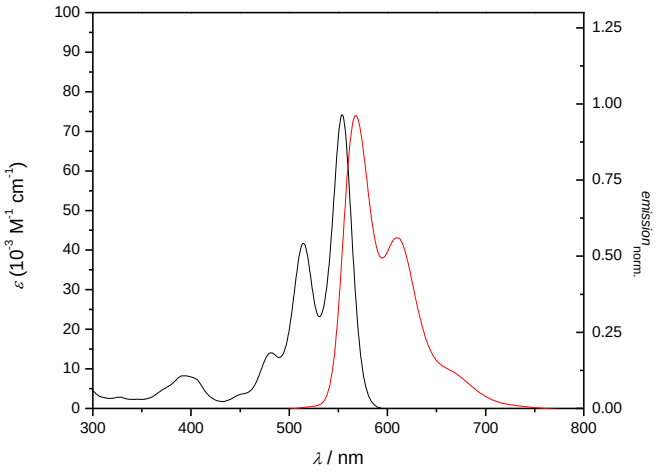

Fig. S7 UV/Vis absorption and emission spectra (both at a concentration of 4.0×10^{-6} M) of PBI **4e** in dichloromethane at room temperature.

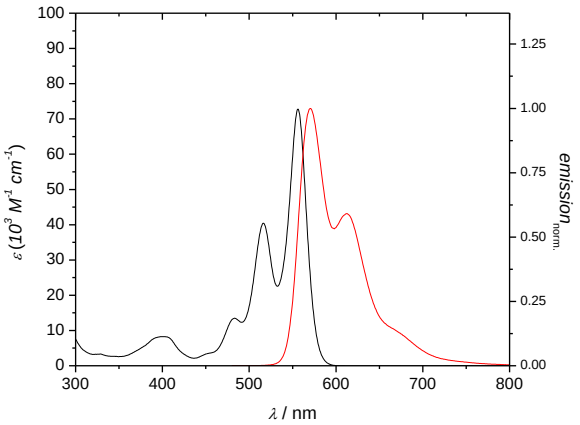

Fig. S8 UV/Vis absorption and emission spectra (both at a concentration of 4.0×10^{-6} M) of PBI **4f** in dichloromethane at room temperature.

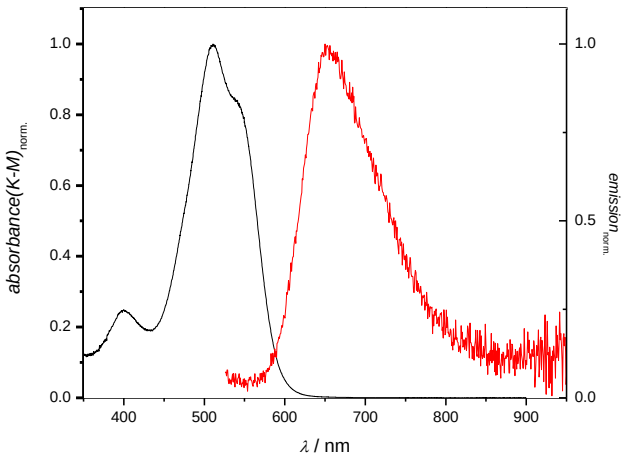

Fig. S9 Solid state absorption and emission spectra of PBI **4b** at room temperature.

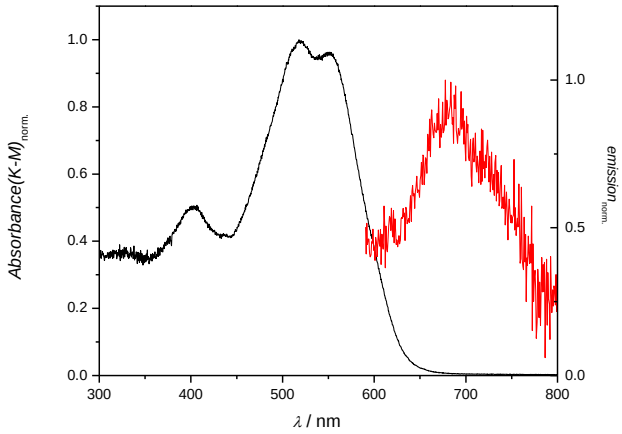

Fig. S10 Solid state absorption and emission spectra of PBI **4c** at room temperature.

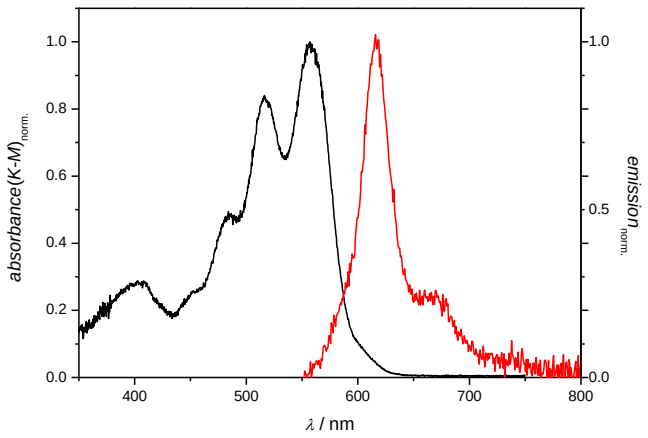

Fig. S11 Solid state absorption and emission spectra of PBI **4d** at room temperature.

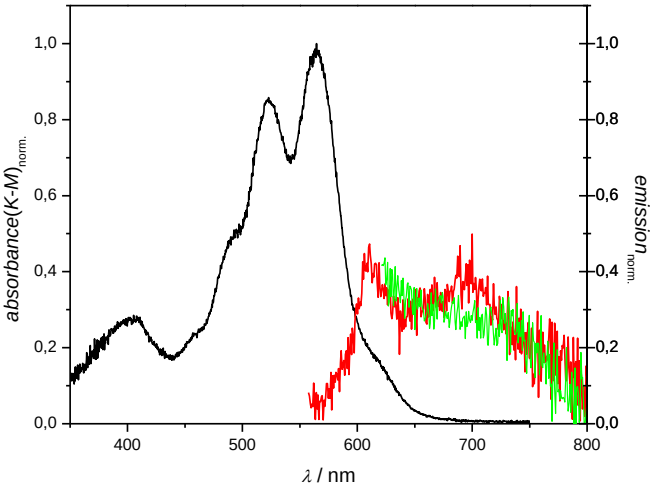

Fig. S12 Solid state absorption and emission spectra of solvent-free crystal of PBI **4e** at room temperature. In green the fluorescence spectrum of **4e** from crystals where one molecule of PBI crystallizes per 0.898 molecules of CH_2Cl_2 is shown.

5. Theoretical Calculation Details

5.1 Calculation of the potential energy curves (PECs)

The potential energy curves were calculated on the assumption of C_2 symmetry. The assumption of C_2 symmetric molecular structures were tested by geometry optimizations without any symmetry constraint starting from the minima of the PECs. For the three studied compounds the minima structures determined without symmetry deviate at most by 0.02° from the C_2 symmetric structure for the studied dihedral angle. The energetic differences between both structures are in the order of 10^{-3} kJ mol^{-1}, which is below the accuracy of the employed DFT method. In order to validate the DFT results, we computed the PECs for **4a** and **4g** using the more accurate RI-SCS-MP2/cc-pVTZ level of theory (Table 3).[S5]

Table S1. Characterization of the ∠(C12a-C13a-C13b-C12b) bending potentials for PBI **4a** and **4g** using SCS-CC2/cc-pVTZ.

PBI	∠(C12a-C13a-C13b-C12b) (°) SCS-MP2	Energy required for planarization (kJ mol^{-1}) SCS-MP2
4a	0.0	0.00
4g	7.3	3.6

5.2 Molecular dynamics (MD) simulations

MD simulations were performed to get a more detailed look into the rotational degree of freedom and the dependencies between ∠(C12b-C1-O-C14) and ∠(C1-O-C14-C15). Simulations were performed for PBIs **4b**, **4c** and **4d**, respectively. All simulations contained 100.000 timesteps of 1 femtosecond each, from which the first 20.000 steps were

used to equilibrate the system. The simulations were performed at 300 K using a Nose-Hoover thermostat. All calculations were carried out with the in-house CAST program. Recent investigations showed that common force fields are too inaccurate, whereas DFT computations are far too expensive. For this reason the simulations were based on the PM6-DH2 method by employing an interface between CAST and the MOPAC program.

5.3 Restricted geometry optimizations

An indirect influence of the packing can occur if the planarity of inner π-conjugated PBI core is induced by the orientations of the outer lying substituents which themselves are determined by packing effects. Since DFT calculations of whole crystals, including periodic boundary conditions, are far too expensive or even not possible, we performed restricted geometry optimizations to somewhat include the influence of the orientations of the outer lying substituents. The orientation of the substituents themselves is determined by packing effects. The starting geometries were based on the X-ray structures of the crystals taken from experiments. For structure **4e** the data obtained by co-crystallization with CH_2Cl_2 was taken.

For the restricted geometry optimizations the positions of all non-hydrogen atoms (oxygen and carbon) of the bay substituents were fixed. The hydrogen atoms of the substituents were allowed to relax, since hydrogen atoms are strictly connected to the heavier centers, and the X-ray data provide no clear data about the positions. Furthermore, no restrictions were applied to the rest of the system. All calculations were performed using BLYP-D3(BJ).

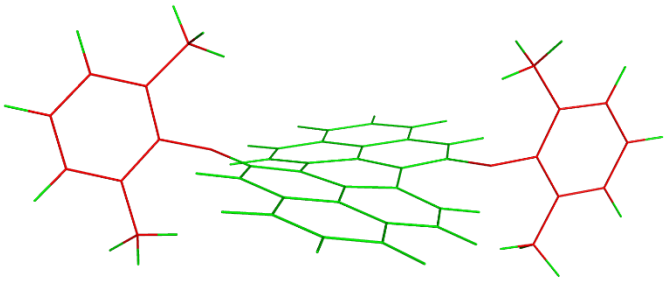

Fig. S13 Ilustrative example for the restricted geometry optimizations of molecule **4d**. The red atoms were fixed in space during the optimization, while the green atoms were allowed to relax. Starting point for each **optimization** was the respective crystal structure.

6. ^{1}H and ^{13}C NMR Spectra of PBIs

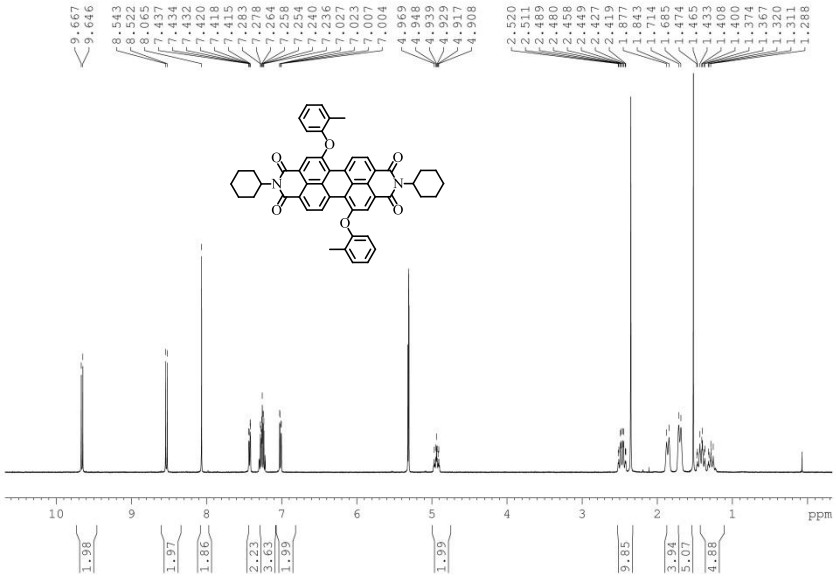

Fig. S14 ^{1}H NMR (400 MHz, CD_2Cl_2, 298 K) of PBI **4c**.

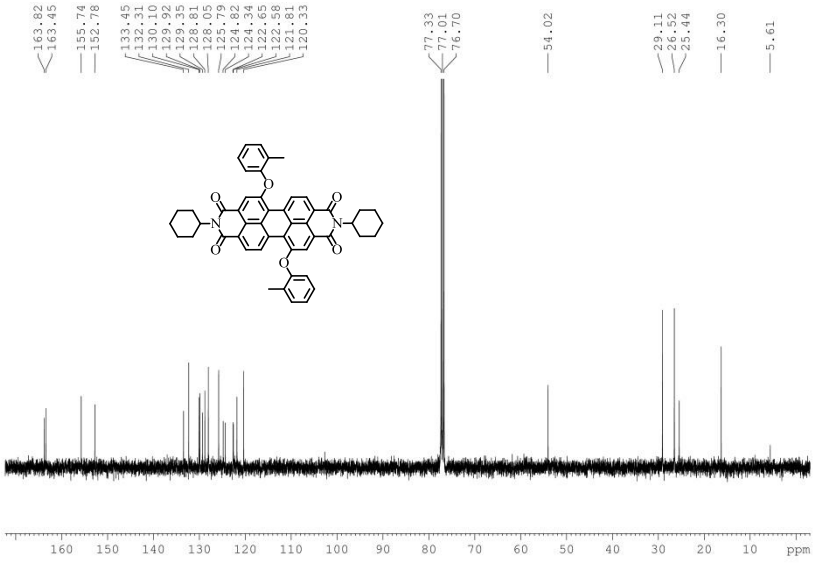

Fig. S15 ^{13}C NMR (100 MHz, $CDCl_3$, 298 K) of PBI **4c**.

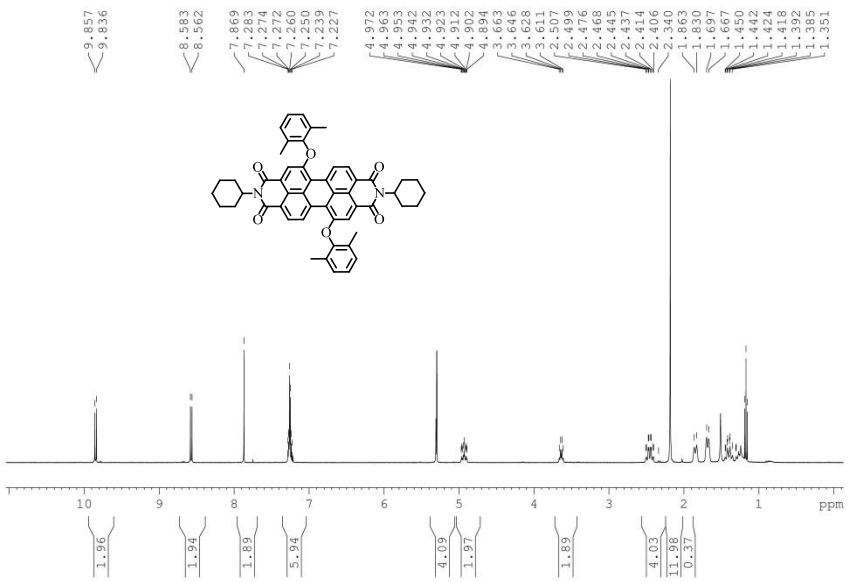

Fig. S16 ^{1}H NMR (400 MHz, CD_2Cl_2, 298 K) of PBI **4d**.

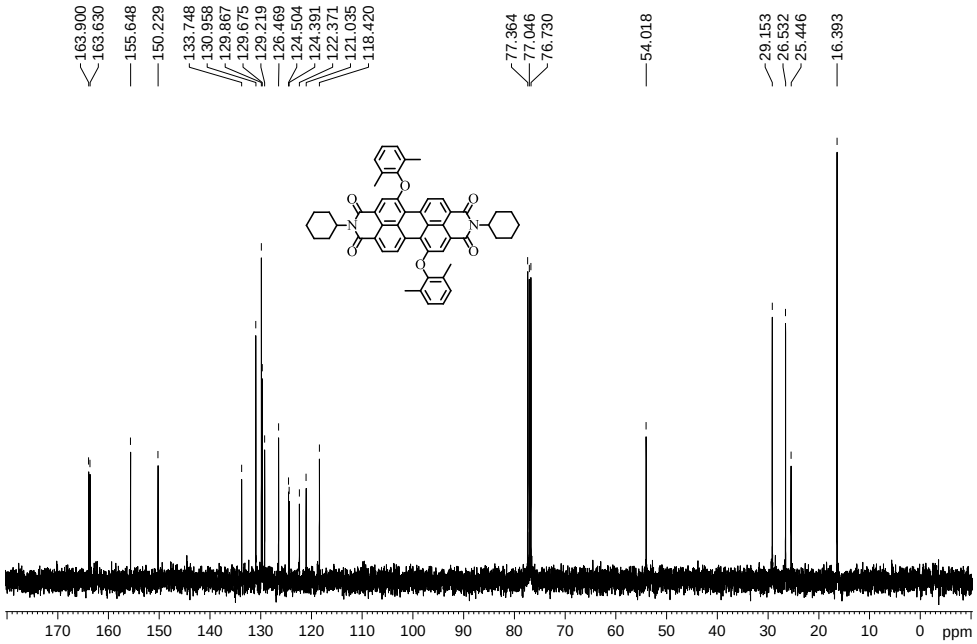

Fig. S17 ^{13}C NMR (100 MHz, $CDCl_3$, 298 K) of PBI **4d**.

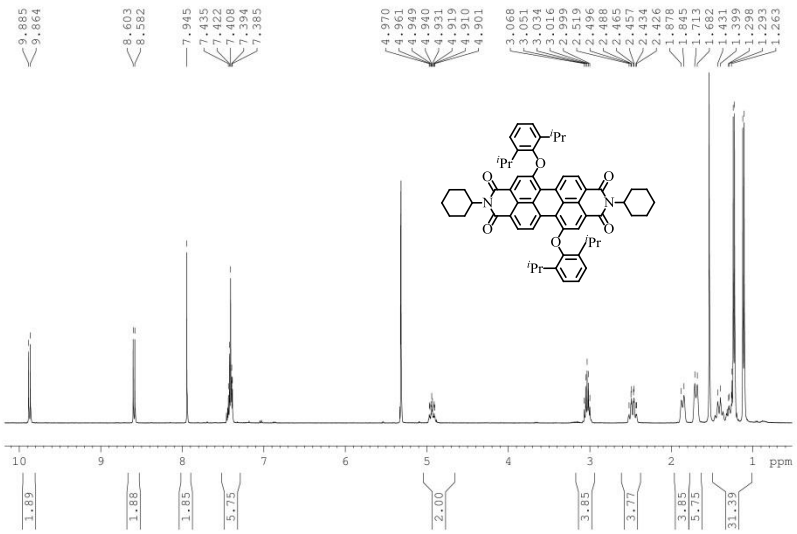

Fig. S18 ^{1}H NMR (400 MHz, CD_2Cl_2, 298 K) of PBI **4e**.

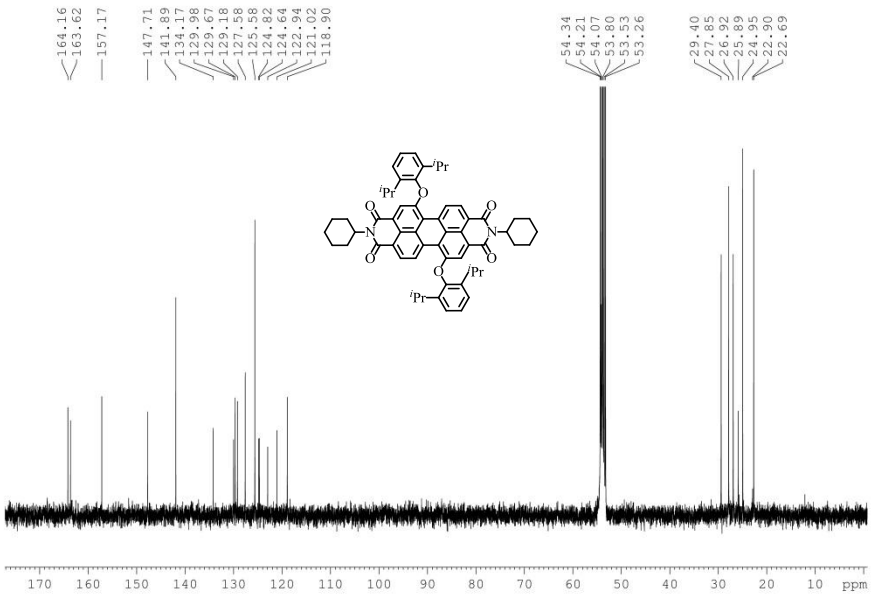

Fig. S19 ^{13}C NMR (100 MHz, CD_2Cl_2, 298 K) of PBI **4e**.

7. References

S1. (*a*) F. Würthner, V. Stepanenko, Z. Chen, C. R. Saha-Möller, N. Kocher and D. Stalke, *J. Org. Chem.*, 2004, **69**, 7933-7939; (*b*) Y. Che, X. Yang, K. Balakrishnan, J. Zuo and L. Zang, *Chem. Mater.*, 2009, **21**, 2930-2934; (*c*) M.-J. Lin, A. J. Jiménez, C. Burschka and F. Würthner, *Chem. Commun.*, 2012, **48**, 12050-12052.

S2. (*a*) R. Sens and K. H. Drexhage, *J. Luminescence*, 1981, **24**, 709-710; (*b*) R. Gvishi, R. Reisfeld and Z. Burshtein, *Chem. Phys. Lett.*, 1993, **213**, 338-344.

S3. G. Sheldrick, *Acta Cryst.*, 2008, **A62**, 112-122.

S4. (*a*) A. L. Spek, *Acta Cryst.*, 2009, **D65**, 148-155; (*b*) A. L. Spek, *J. App. Crystallogr.*, 2003, **26**, 7-13; (*c*) P. van der Sluis and A. L. Spek, *Acta Crystallogr., Sect. A*, 1990, **46**, 194-201.

S5. (*a*) C. Hättig, *J. Chem. Phys.*, 2003, **118**, 7751-7761; (*b*) A. Hellweg, S. A. Grün and C. Hättig, *Phys. Chem. Chem. Phys.*, 2008, **10**, 4119-4127.